https://doi.org/10.1016/j.ymssp.2018.12.017

Baseline-free adaptive damage localization of plate-type structures by using robust PCA and Gaussian smoothing

Shancheng Cao[1], Huajiang Ouyang[2] and Li Cheng[1,*]

[1]Department of Mechanical Engineering, The Hong Kong Polytechnic University, Kowloon, Hong Kong, China
[2]Centre for Engineering Dynamics, School of Engineering, The University of Liverpool, Liverpool, L69 3GH, U.K.

Abstract

Damage localization in plate-type structures has been widely investigated by exploring the structural characteristic deflection shapes (CDS's) or their spatial derivatives. Despite the substantial advances in this kind of methods, several key issues still need to be addressed to boost their efficiency for practical applications. This study considers three essential problems: susceptibility to measurement noise, absence of baseline-data on pristine structures, and selection of measurement sampling interval and that of the parameters to be used in the de-noising techniques for more accurate damage localization. To tackle these problems, a novel baseline-free adaptive damage localization approach is proposed, which combines the robust Principal Component Analysis (PCA) with Gaussian smoothing. A damage localization evaluator is defined to determine both the spatial sampling interval of the CDS's and the scale parameter of Gaussian smoothing to warrant a better damage localization. Moreover, effects of the measurement noise and numerical errors due to the use of the finite difference scheme on the estimate of the CDS derivatives are quantified. Finally, the feasibility and the effectiveness of the proposed method are verified both numerically and experimentally by using a cantilever plate with a small damage zone. It is found that the second-order spatial derivative of the CDS's is able to provide the best damage localization results among the first four order spatial derivatives of the CDS's.

* Corresponding author, email address: li.cheng@polyu.edu.hk

Keywords: Damage localization, structural characteristic deflection shape, robust principal component analysis, Gaussian smoothing, finite difference method

1 Introduction

Vibration-based methods for the detection and localization of structural damage play a significant role in structural health monitoring and have experienced a rapid development in the past several decades [1-5]. Recently, damage identification in plate-type structures has attracted more attention [6-8]. As compared to natural frequencies, structural characteristic deflection shapes (CDS's) or their spatial derivatives are more effective and sensitive dynamic features, as structural damage is typically a local phenomenon that initiates and propagates within a local area [9, 10]. Here, the so-called structural characteristic deflection shapes refer to spatial shape-type features, e.g., mode shapes and operational deflection shapes [11, 12]. Moreover, CDS-based damage identification methods tend to be much more robust to environmental and operational variability than natural frequency-based methods. With the development of advanced measurement techniques like scanning laser vibrometer (SLV) or full-field digital image correlation, CDS's can be readily acquired at a high spatial resolution within a short time. However, CDS's and their spatial derivatives are vulnerable to measurement uncertainties. For example, the CDS's acquired by a SLV are easily contaminated by speckle noise [13].

The CDS- or its spatial derivative-based damage localization methods can either be baseline-based or baseline-free. In practice, baseline data on pristine structures may not be available. Therefore, baseline-free methods which only utilize CDS's or CDS spatial derivatives of the damaged state are more attractive and useful. To examine the damage-induced local characteristics without baseline data, advanced signal processing methods are commonly used, exemplified by methods like wavelet analysis or fractal dimension analysis [14-16]. Gentile and Messina [17] studied the Gaussian wavelet transforms in

localizing open cracks of beams and concluded that high-order Gaussian derivative wavelets were more sensitive to damage. Cao and Qiao [18] employed the stationary wavelet transform to improve the noise robustness of mode shapes and applied continuous wavelet transform to localize the damage. Bai *et al.* [19] applied fractal dimension analysis to high-order mode shapes of plates based on the fractal surface singularities. Moreover, fractal dimension analysis could be combined with wavelet analysis to enhance the noise robustness of damage localization [20]. A common limitation of this kind of methods, however, is to the difficulty in integrating the damage information of several CDS's or CDS spatial derivatives for robust damage localization.

On the other hand, without the baseline data on pristine structures, the pseudo-CDS's or CDS spatial derivatives of the undamaged state are primarily constructed based on those of the damaged state by surrogate models or low-rank models (such as principal component analysis (PCA)) [21, 22]. Then, differences in CDS's or CDS spatial derivatives between the damaged state and the undamaged state are evaluated to localize the damage. The basic principle is that the CDS's or CDS spatial derivatives of an intact plate are smooth; or, when represented as a matrix by following the measurement grid, possess a low-rank structure. Xu and Zhu [23] employed a polynomial fitting approach to construct the mode shapes of the undamaged plates. The square of the absolute differences with mode shapes of the damaged plates was then used for damage localization. Cao and Ouyang [24] proposed a robust damage localization index by incorporating the damage information of several modes, which applied gapped smoothing method to extract the damage characteristics of mode shapes. Yang *et al.* [25] investigated the low-rank and sparse data structure of a 2-D strain field for damage identification in plates. One advantage of this kind of methods is that the damage-induced local shape characteristics can be clearly extracted. Furthermore, the extracted damage features of several CDS's or CDS spatial derivatives can be readily integrated for robust damage localization.

Generally speaking, high-order spatial derivatives of the CDS's, especially the curvature, are commonly used for structural damage localization in flexible structures, as the spatial derivatives can effectively amplify the damage-induced local structural changes [26-28]. However, the finite difference method, usually adopted for estimating the spatial derivatives of CDS's, spreads and amplifies the numerical and measurement errors, which can severely degrade the estimation accuracy of these quantities [29]. To tackle the problem, two strategies, namely the proper choice of the sampling interval and low-pass filters, are commonly used [30-32]. For the former, a numerical solution was presented by Sazonov and Klinkhachorn [31] to minimize the effect of the measurement noise and that of the truncation errors of the finite element method on the calculation of the curvature and strain energy mode shapes. For the latter, methods including cubic spline interpolation [33], wavelets [34], Gaussian function derivatives [35] and wavenumber filtering [36] were investigated. However, these damage localization strategies cannot guarantee the best (the most accurate) damage localization result.

This paper proposes a novel baseline-free adaptive damage localization method to achieve the best damage localization by using only CDS's or their spatial derivatives of the damaged state. The proposed method takes advantage of the low-rank structure of 2-D CDS's and the sparse property of the structural damage locations. Different from the methods that intuitively setting the measurement sampling interval and the denoising parameters, a damage localization evaluator (DLE) is defined to quantify the damage localization performance and to determine the optimal spatial measurement sampling interval and the proper scale parameter of Gaussian smoothing for the best damage localization corresponding to the highest DLE value. In addition, localization results using the first four order spatial derivatives of the CDS's are presented and compared to evaluate the proper order of the CDS spatial derivatives for more accurate damage localization.

The structure of the paper is organized as follows. In Section 2, the principle of damage localization of plates by using CDS's or CDS spatial derivatives is described and a baseline-free damage localization index is defined based on a robust PCA. Then, the noise propagation and truncation errors of the finite element method during high-order CDS spatial derivative estimation are quantified in Section 3. In Section 4, an adaptive damage localization method is proposed and a damage localization evaluator is defined. Numerical and experimental studies are then conducted to verify the proposed approach in Section 5 and Section 6, respectively. Finally, conclusions are summarized in Section 7.

2 Principle of the baseline-free damage localization in plates

Consider a homogeneous and isotropic thin plate of constant thickness h. The governing equation of harmonic motion at a given angular frequency ω writes

$$D\nabla^2\nabla^2 w(x,y) + \mathrm{j}C\omega w(x,y) - \rho h\omega^2 w(x,y) = f(x,y) \tag{1}$$

where $\mathrm{j}=\sqrt{-1}$; $\nabla^2 = \partial^2/\partial x^2 + \partial^2/\partial y^2$ is the Laplace operator; $D = Eh^3/\left(12(1-\upsilon^2)\right)$ is the plate's flexural rigidity with Young's modulus E and the Poisson's ratio υ. $w(x,y)$ denotes the plate displacement in the z-direction; C indicates the viscous damping coefficient and ρ the mass density.

If the external force distribution $f(x,y)$ and its spatial derivatives are always continuous including $f(x,y)=0$, the damage-induced changes in Young's modulus E or plate thickness h will cause a sudden change/singularity in $w(x,y)$ and then $w_{\mathrm{d}}(x,y)$ (d indicates the damaged state) can be used for damage detection and localization.

Traditionally, the high-order spatial derivatives of $w_{\mathrm{d}}(x,y)$ are preferred, as they are more sensitive to incipient damage than $w_{\mathrm{d}}(x,y)$ [28]. To extract the damage-induced features in $w_{\mathrm{d}}^r(x,y)$ ($w_{\mathrm{d}}^r(x,y) = (\partial^r/\partial x^r + \partial^r/\partial y^r)w_{\mathrm{d}}(x,y)$, $\forall r \in [0,+\infty]$ and r is an integer), a robust principal component analysis is adopted, which decomposes $\mathbf{W}_{\mathrm{d}}^r$($\mathbf{W}_{\mathrm{d}}^r \in \mathbb{R}^{n_1\times n_2}$ is a matrix containing $w_{\mathrm{d}}^r(x,y)$ at all measurement points) into a low-rank matrix **L**, a sparse matrix **DI** (which is defined as the damage index matrix

for damage localization) and a noise matrix **E** as

$$\begin{gathered}\mathbf{W}_{\mathrm{d}}^{r}=\mathbf{L}+\mathbf{DI}+\mathbf{E}\\ \text{minimize } \|\mathbf{L}\|_{*}+\xi\|\mathbf{DI}\|_{1} \text{ subject to } \|\mathbf{W}_{\mathrm{d}}^{r}-\mathbf{L}-\mathbf{DI}\|\leq\epsilon\end{gathered} \tag{2}$$

where $\xi>0$ is an arbitrary balance parameter; ϵ $(\epsilon>0)$ a threshold for noise matrix **E**. $\|\mathbf{L}\|_{*}=\sum_{i}\lambda_{i}(\mathbf{L})$ represents the nuclear norm of matrix **L** (which is the ℓ_1 norm of singular values) and $\|\mathbf{DI}\|_{1}=\sum_{ij}|DI_{ij}|$ denotes the ℓ_1 norm of matrix **DI**. The healthy state $w^{r}(x,y)$ can be well approximated by **L** and the damage-induced changes/singularities in $w_{\mathrm{d}}^{r}(x,y)$ are revealed by **DI**.

Moreover, the balance parameter ξ in Eq. (2) should be properly chosen to well separate the low-rank matrix **L** and the sparse matrix **DI**. It can be seen that an **L** with a sufficiently high rank will incorporate the damage features in its representation. For a very low rank **L**, however, characteristic deflection shape features will be embedded in **DI**, which will corrupt the damage identification procedure and even produce misleading identification results. Here, $\xi=1/\sqrt{\max(n_1,n_2)}$ is chosen based on the work reported in the related papers [37, 38].

3 Problems in high-order derivative estimation

The spatial derivatives of $w(x,y)$, $w^{r}(x,y)$, such as slopes ($r=1$), curvatures ($r=2$) and, more recently, third and four derivatives, have been widely used to localize damage in plate-type structures due to their damage sensitivity [39]. The most used approach to evaluate $w^{r}(x,y)$ is via the finite difference method, thus generating two essential problems: noise propagation and numerical approximation, which may jeopardize the accurate damage localization.

3.1 Noise propagation of the finite difference method

The acquired displacement $w(x,y)$ can be easily contaminated by measurement noise. To mathematically demonstrate the uncertainty propagation due to the finite difference calculation, $w(x,y)$ is assumed to be polluted by Gaussian white noise as

$$\widetilde{w}(x,y)=w(x,y)+n(x,y) \tag{3}$$

in which $n(x,y)$ is the Gaussian white noise and expressed in detail as

$$n(x,y)=n_{\mathrm{level}}n_{\mathrm{n}}\sigma_{w} \tag{4}$$

where n_{n} denotes the normally distributed random white noise with a zero-mean with a variance being 1; n_{level} is the noise level range of [0, 1] and σ_w the standard variance of $w(x,y), \forall x,y$. Thus, the mean value and standard deviation of $n(x,y)$ are 0 and $\sigma_{\mathrm{n}} = n_{\mathrm{level}}\sigma_w$, respectively.

Taking the spatial derivative estimation along x direction as an example, the uncertainty propagation at each measurement point writes

$$E_{\mathrm{n}}^{r} = \frac{\partial^r \tilde{w}(x_i,y_j)}{\partial x^r} - \frac{\partial^r w(x_i,y_j)}{\partial x^r} = \sum_{k=-m}^{m} c_k\, n\left(x_{i+k}, y_j\right)/d_x^r \tag{5}$$

where c_k is the coefficient of the finite difference method and the coefficients of the second-order central difference method are tabulated in Table 1. $n\left(x_{i+k}, y_j\right)$ is an independent random variable for different k and possesses the same probability distribution of $(0, \sigma_{\mathrm{n}})$. In addition, d_x denotes the spatial sampling interval of $w(x,y)$ along x direction.

Table 1. Coefficients of the central differences with second-order accuracy.

r	c_{-2}	c_{-1}	c_0	c_1	c_2	c^r
1		-1/2	0	1/2		1/6
2		1	-2	1		1/12
3	-1/2	1	0	-1	1/2	1/4
4	1	-4	6	-4	1	1/6

In Eq. (5), E_{n}^{r} still holds a normal distribution with the mean value and standard deviation being 0 and $\sqrt{\sum_{k=-m}^{m} c_k^2}\,\sigma_{\mathrm{n}}/d_x^r$, respectively. It can be seen that the finite difference method significantly amplifies the effects of the measurement noise in high-order spatial derivatives $w_{\mathrm{d}}^{r}(x,y)$, as d_x is normally very small during experimental measurements. Moreover, the higher the order of $w_{\mathrm{d}}^{r}(x,y)$, the more sensitive it is to the measurement noise.

3.2 Truncation errors of the finite difference method

Truncation errors are caused by the difference between the actual solution and the approximate solution [40]. The principle of the finite difference scheme is a Taylor expansion in which a truncated series are typically used instead of an infinite series.

Taking the x coordinate as an example, $w\left(x_{i+1}, y_j\right)$ is expressed at $x = x_i$

according to linear Taylor expansion as

$$w(x_{i+1}, y_j) = w(x_i, y_j) + \cdots + \frac{d_x^r}{r!}\frac{\partial^r w(x_i, y_j)}{\partial x^r} + \frac{d_x^{r+1}}{(r+1)!}\frac{\partial^{r+1} w(\xi_x, y_j)}{\partial x^{r+1}}, \xi_x \in [x_i, x_{i+1}] \quad (6)$$

Based on Eq. (6), the truncation error at each measurement point is evaluated by

$$E_{\mathrm{t}}^r = c^r d_x^2 \frac{\partial^{r+2} w(\xi_x, y)}{\partial x^{r+2}}, \ \xi_x \in [x_{-m}, x_m] \quad (7)$$

in which, c^r is the coefficient and its value for the second-order central difference method is tabulated in the last column of Table 1. Moreover, Eq. (7) indicates that the truncation errors are proportional to the square of the spatial sampling interval d_x and the two-order higher derivative of the estimated derivatives.

By increasing d_x, the truncation error E_{t}^r tends to be amplified whilst the noise effect E_{n}^r being reduced accordingly, which is typically depicted in Fig. 1. In general, an optimal d_1 can be obtained to minimize the average total errors of measurement noise and truncation errors for a given order r. However, it is not realistic to determine the optimal d_1 without the priori information on measurement noise. Furthermore, the optimal d_1 does not set the damage localization performance as the direct optimization objective. To address this issue, an alternative strategy is proposed, which optimizes the damage localization performance by adjusting the measurement sampling interval after an initial high spatial resolution measurement. Furthermore, at a given measurement sampling interval d, the scale parameter σ of Gaussian smoothing will be tuned to obtain the optimal damage localization.

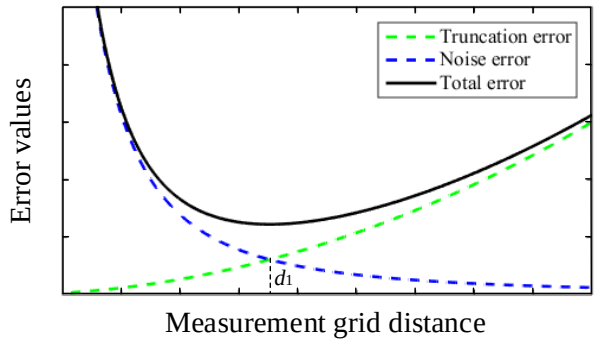

Figure 1. Typical plot of the total errors of the finite difference method.

4 Adaptive damage localizations in plates

4.1 Damage localization evaluator

In order to obtain the best damage localization results by exploring a given measurement data set, a damage localization evaluator is defined to quantify the damage identification performance. Then, the best damage localization is achieved by adaptively adjusting the spatial sampling interval d and the scale parameter σ of Gaussian smoothing which warrant the highest DLE value. DLE is defined as

$$DLE = h_1/h_2 \tag{8}$$

where h_1 and h_2 denote the peak values of **DI** within and outside the damage zone, respectively, which are shown in Fig. 2(a). As the area of the damage zone is unknown *a priori*, an equivalent estimation zone (EEZ) is assumed, which is illustrated in Fig. 2(b). In the present case, the maximum absolute outlier value in **DI** is chosen as the centre of the EEZ, which is set as 0.05×0.05 m^2.

While the centre of the EEZ can be easily determined, its area should be properly set which indeed needs careful considerations. Theoretically and ideally, the area of EEZ should be larger than the actual damage zone to completely remove the damage effects on areas outside EEZ, as the establishment of **DI** involves neighbouring measurement points beyond the damaged zone. Furthermore, a large-scale parameter σ of Gaussian smoothing will enlarge the damage zone as well. In practice, without knowing the actual size of the damage, one can start with a relatively large EEZ as long as the areas outside EEZ are still able to reflect the characteristics of measurement noise (noise-induced outlier values randomly scattered over the plate surface). If the noise-induced characteristics are not detected, the area size of EEZ could be successively reduced until these are detected.

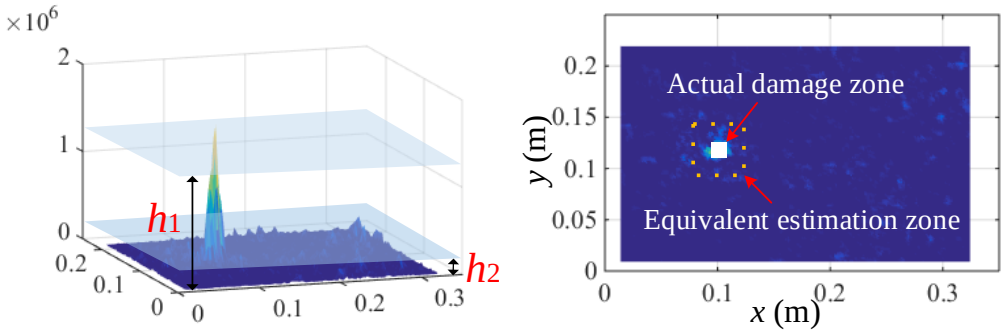

(a) (b)

Figure 2. Definition of (a) damage localization evaluator (DLE) and (b) equivalent estimation zone (EEZ).

4.2 Adjustment of measurement sampling interval

Initially, a smaller sampling interval d is used during the data acquisition phase. Then, d will be adjusted by a triangulation-based linear interpolation. In the process, the observation points are discretized into Delaunay triangulation and a neighbourhood of nearby measurement points are used for the linear interpolation.

Linearly interpolating the planar surface of a triangle only requires applying barycentric coordinates to the data at the vertices of the triangle. This is a weighted average method and the value of the interpolated surface $\widehat{w}_{\mathrm{d}}(x,y)$, at any interpolation point (x,y) within the triangle is

$$\widehat{w}_{\mathrm{d}}(x,y) = \sum_{i=1}^{3} \theta_i \; w_{\mathrm{d}}(x_i,y_i) \tag{9}$$

where the coefficient θ_i is the ith barycentric coordinate of the interpolation point with respect to the triangle; and $w_{\mathrm{d}}(x_i,y_i)$ the observed value at the data point (x_i,y_i).

4.3 Gaussian smoothing

Since the high-order spatial derivative estimation is very susceptible to the measurement noise, it is common to smoothen $w_{\mathrm{d}}(x,y)$ before applying the finite difference method. To this end, a Gaussian smoothing is applied, which convolves $w_{\mathrm{d}}(x,y)$ with a Gaussian function as

$$\widehat{w}_{\mathrm{d}}(x,y;\sigma) = \int_{-l}^{+l}\int_{-l}^{+l} w_{\mathrm{d}}(x-u,y-v)g(u,v;\sigma)\,dudv \tag{10}$$

where σ denotes the scale parameter and $g(x,y;\sigma)$ is a two-dimension Gaussian function and expressed as $1/(2\pi\sigma^2)\exp^{(-(x^2+y^2)/(2\sigma^2))}$. In addition, the size of the Gaussian smoothing is limited to a window of $[-l,l]$ instead of $[-\infty,+\infty]$. Here, $l=\lceil 3\sigma \rceil$ is used to approximate 99.73% of the Gaussian kernel, where $\lceil 3\sigma \rceil$ represents the ceil of 3σ. It is seen that the window size is a function of the scale parameter σ of Gaussian function. Therefore, when optimizing σ, the window size will be tuned accordingly.

Due to the differentiation property of the convolution integral, the rth-order spatial derivative of $\widehat{w}_{\mathrm{d}}(x,y;\sigma)$ can be calculated in two equivalent forms as

$$\widehat{w}_{\mathrm{d}}^{r}(x,y;\sigma)=w_{\mathrm{d}}(x,y)\otimes g^{r}(x,y;\sigma)=w_{\mathrm{d}}^{r}(x,y)\otimes g(x,y;\sigma) \tag{11}$$

in which, $\otimes$ represents the convolution operator described in Eq. (10).

By adjusting σ, $\widehat{w}_{\mathrm{d}}^{r}(x,y;\sigma)$ can be handled at different spatial scales. It is well known that the damage-induced outlier values in **DI** tend to be spatially close to each other whilst the noise-caused outlier values tend to be scattered over the measured plate surface, which are depicted in Fig. 3(a). For a smaller σ, there will be many outlier values due to measurement noise as shown in Fig. 3(a). By increasing σ, fine-scale features will disappear, which include both noise effects and damage-induced local features. For a larger σ, the damage-induced local shape characteristics will be smoothed as well [41]. Thus, an appropriate selection of σ is required to obtain the best damage localization as displayed in Fig. 3(b).

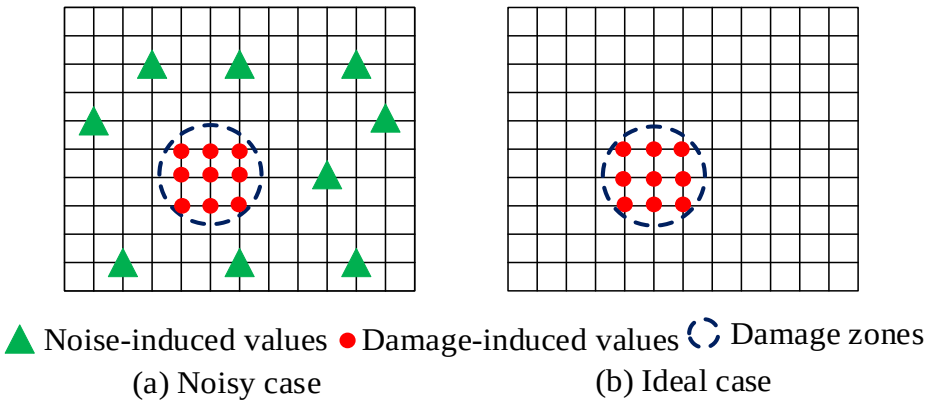

Figure 3. An illustration of damage localization results.

The boundaries imply some discontinuities on the estimated $\widehat{w}_{\mathrm{d}}^{r}(x,y)(r=1,2,3,4)$, which cannot be eliminated by Gaussian smoothing. Moreover, this has to be processed before Gaussian smoothing, as Gaussian smoothing propagates the discontinuity effects of boundaries [42]. Here, a spatial Hanning window is applied to $w_{\mathrm{d}}^{r}(x,y)$ before Gaussian smoothing. The 2-D window is defined by the product of two identical 1-D windows [43] as

$$\varphi_{2\mathrm{D}}(x,y)=\varphi(x)\varphi(y) \tag{12}$$

in which, $\varphi(x)$ is defined by

$$\begin{cases} \varphi(x)=1/2\big(1-\cos(\pi x/\alpha)\big), x\in[0,\alpha] \\ \varphi(x)=1, x\in(\alpha, L_x-\alpha) \\ \varphi(x)=1/2\big(1-\cos(\pi(x-L_x+2\alpha)/\alpha)\big), x\in[L_x-\alpha, L_x] \end{cases} \tag{13}$$

The value of α denotes the width on the boundary of $w_{\mathrm{d}}^{r}(x,y)$ where the spatial derivatives are discontinuous. As shown in Table 1, one measurement point for the first and second order derivatives and two measurement points for the third and fourth-order derivatives cannot be used. In this paper, α is set as the length of the first five measurement points around the boundaries to further suppress the effects of boundaries.

Finally, the proposed baseline-free adaptive damage localization method is illustrated by the flowchart in Fig. 4.

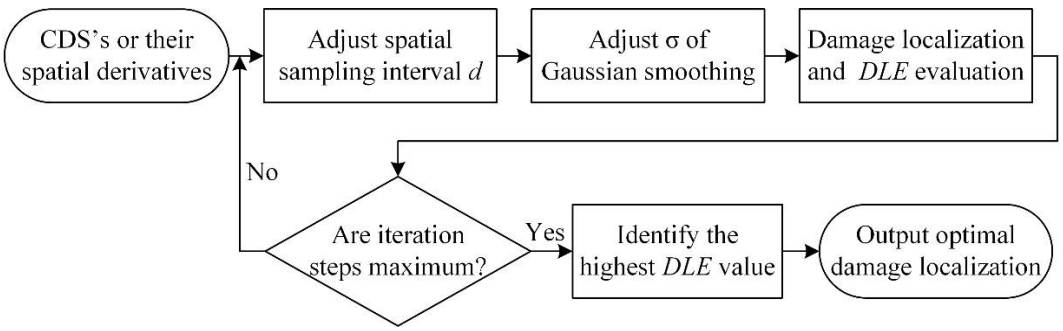

Figure 4. A flowchart of the proposed baseline-free adaptive damage localization.

5 Numerical studies

A cantilever aluminium plate, of a dimension $0.35 \times 0.23 \times 0.003$ m^3 with Young's modulus E=69 GPa, Poisson's ratio $\nu = 0.35$ and mass density ρ=2700 kg/m^3, is studied. The plate is modelled using the four-node quadrilateral elements in MATLAB according to the Mindlin plate theory. The cantilever plate, clamped on the left, is discretized into 140×92 elements with an element size of $0.0025 \times 0.0025 \times 0.003$ m^3. The plate contains a damage zone of 0.02×0.02 m^2, which is centred at (0.10m, 0.115m) as graphed in Fig. 5(a). The damage is simulated by reducing the plate thickness of the associated finite elements.

In the following study, the 10th mode shape is used as a representative example, which is shown in Fig. 5(b). The main purpose here is to demonstrate the working principle and the feasibility of the proposed adaptive damage localization based on robust PCA. In practical applications, different mode shapes show different sensitivities to damage at different locations and each one has its own blind inspection zones such as the areas around the nodes of the mode shape. Therefore, the damage information from more mode shapes should be integrated to warrant a more robust and reliable damage localization. As one of the options, the proposed **DI** in Eq. (2) can be readily embedded into a data fusion approach to combine the damage localization results based on different mode shapes [44].

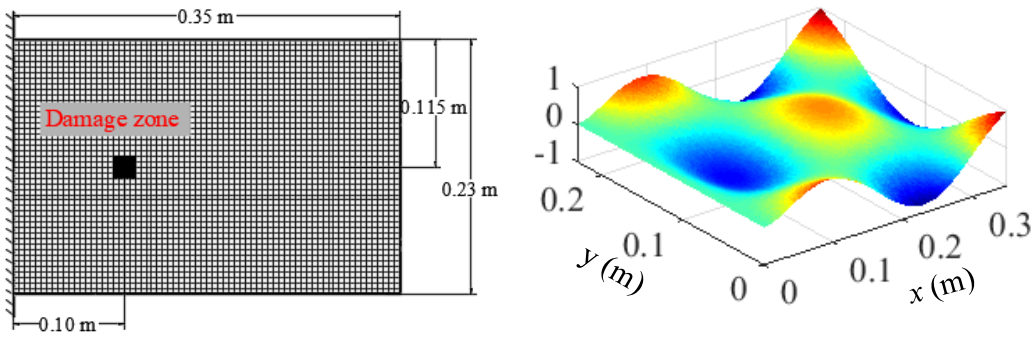

(a) (b)

Figure 5. (a) FE model of a plate with a damage zone and (b) the 10th mode shape.

In this numerical study, the noise-free damage localization results of the plate with a damage of 5% depth reduction are first presented in Fig. 6 to verify the effectiveness of

the proposed **DI** in Eq. (2).

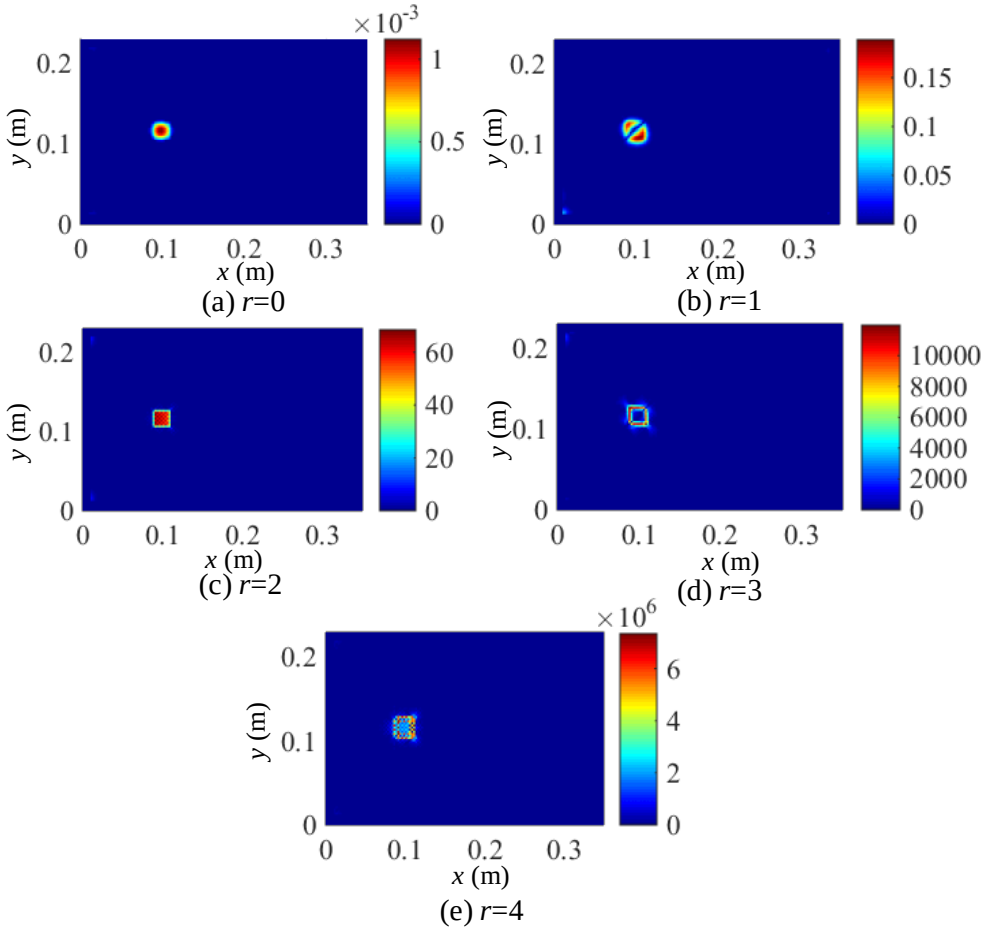

Figure 6. Noise-free damage localization results using $w_{\mathrm{d}}^{r}(x,y)(r=0,1,2,3,4)$

It is seen from Fig. 6 that the damage zone is clearly identified by using either the mode shape or any of its first four spatial derivative terms, regardless of the magnitude level of the **DI**. Thus, the robust PCA is proved to be powerful in extracting the damage-induced local shape features in plate-type structures. Moreover, the higher the order of $w_{\mathrm{d}}^{r}(x,y)$, the larger the magnitude of the damage-induced local shape discontinuities. Hence, the high-order spatial derivatives of $w_{\mathrm{d}}(x,y)$ is able to enhance the local damage characteristics, which naturally boosts structural damage identification. In addition, the extracted damage-induced characteristics of $w_{\mathrm{d}}^{r}(x,y)(r=0,2,4)$ in Figs. 6 (a), (c) and (e) present clear peak features whilst $w_{\mathrm{d}}^{r}(x,y)(r=1,3)$ in Figs. 6 (b) and (d) provide two separated shape features. In practice, the damage-induced features of $w_{\mathrm{d}}^{r}(x,y)(r=1,3)$ may cause misleading damage localization results and this will be illustrated further in the following study.

Secondly, to investigate the effects of measurement noise on $w_{\mathrm{d}}^{r}(x,y)(r=0,1,2,3,4)$, a

Gaussian white noise of n_{level} =0.05% (Signal to noise ratio =66.15 dB) is added to pollute the 10th mode shape and the damage localization results of the plate with the same damage of 5% depth reduction are presented in Fig. 7.

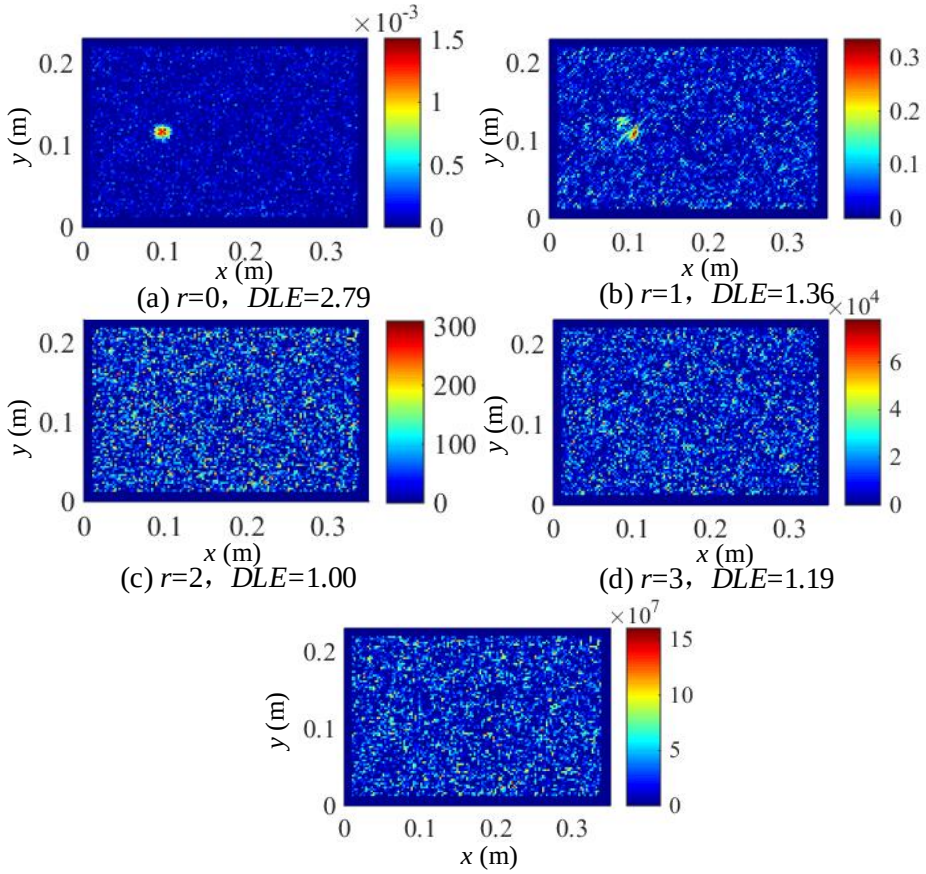

(a) r=0, DLE=2.79 (b) r=1, DLE=1.36

(c) r=2, DLE=1.00 (d) r=3, DLE=1.19

(e) r=4, DLE=1.02

Figure 7. Damage localization results using $w_{\text{d}}^{r}(x,y)(r=0,1,2,3,4)$ with 0.05% noise.

It is clear that the damage localization results using high-order $w_{\text{d}}^{r}(x,y)$ $(r=2,3,4)$ are severely degraded by the added Gaussian white noise, whilst $w_{\text{d}}(x,y)(r=0)$ still provides accurate damage localization results, as shown in Fig. 7(a). Moreover, damage characteristics in $w_{\text{d}}^{r}(x,y)$ $(r=1,2,3,4)$, as displayed in Fig. 6, are overwhelmed by the propagated measurement noise of the finite element method.

To tackle the problem, the spatial sampling interval d of $w_{\text{d}}(x,y)$ and the scale parameter σ of Gaussian smoothing are optimized to obtain the best damage localization results. The DLE values at different sampling interval d and scale parameter σ of $w_{\text{d}}^{r}(x,y)$ $(r=1,2,3,4)$ are shown in Fig. 8.

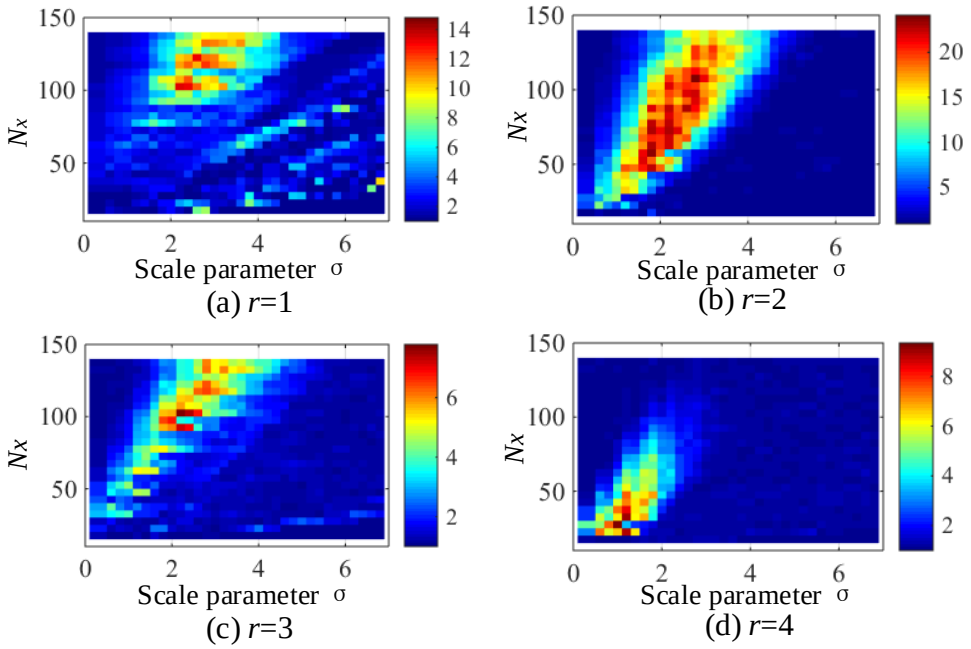

Figure 8. DLE values at different d and σ using $w_{\mathrm{d}}^{r}(x,y)(r=1,2,3,4)$ (N_x is the number of measurement points along x direction, d=0.35/N_x and $N_y=\mathrm{round}(0.23/d)$).

It is seen from Fig. 8 that only a small region of the combined d and σ can provide a large DLE value, corresponding to better damage localization performance. Therefore, it is vital to optimize the sampling interval d and apply proper denoising techniques for accurate damage localization when using high-order derivatives of CDS's. Moreover, $w_{\mathrm{d}}^{2}(x,y)$ is able to provide high DLE values at a wide range of d whilst the $w_{\mathrm{d}}^{4}(x,y)$ only performs well for some large d, which demonstrates that $w_{\mathrm{d}}^{4}(x,y)$ is more prone to measurement noise. In addition, $w_{\mathrm{d}}^{2}(x,y)$ is more sensitive to damage, as it possesses the largest zone of high DEL values and the highest DLE values among $w_{\mathrm{d}}^{r}(x,y)$ $(r=1,2,3,4)$.

To further interpret the damage localization performance at different DLE values in Fig. 8, the damage localization results using different σ for d=0.0025m (N_x=140) is illustrated in Fig. 9. Figures 9 (b) and (d) indicate that the damage localization results are poor for both excessively small and large σ, with DLE values being around 1. Furthermore, by increasing σ, the magnitude of outlier values in **DI** becomes smaller as indicated in Figs. 9(b)-(d), suggesting a reduction in both the noise and damage-

induced singularities. In addition, the identified damage zone in Fig. 9(c) is a circle whilst the original damage zone is a square, which is caused by Gaussian smoothing.

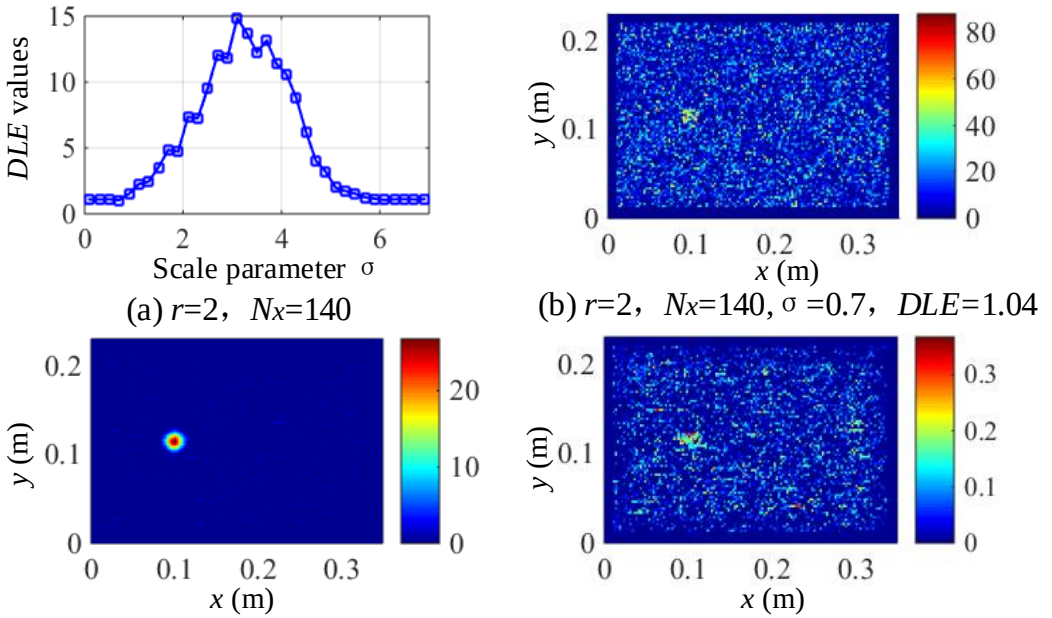

(a) r=2， Nx=140 (b) r=2， Nx=140, σ =0.7， DLE=1.04

(c) r=2， Nx=140, σ =3.1， DLE=14.86 (d) r=2， Nx=140, σ =5.9， DLE=1.14

Figure 9. Damage localization of a plate with a damage of 5% depth reduction by using $w_{\mathrm{d}}^{2}(x,y)$ with 0.05% noise.

Finally, the best damage localization results using $w_{\mathrm{d}}^{r}(x,y)(r=1,2,3,4)$ are presented in Fig. 10. It is clear from Fig. 10 that all the spatial derivatives $w_{\mathrm{d}}^{r}(x,y)(r$=1,2,3,4) can achieve accurate damage localization when using optimal d and σ which correspond to the highest DLE values in Fig.8, while this is impossible by using the original noisy data as shown in Fig. 7. Moreover, $w_{\mathrm{d}}^{2}(x,y)$ and $w_{\mathrm{d}}^{4}(x,y)$ tend to work better for damage localization than $w_{\mathrm{d}}^{1}(x,y)$ and $w_{\mathrm{d}}^{3}(x,y)$, as the latter two provide two damage zones for a single damage location.

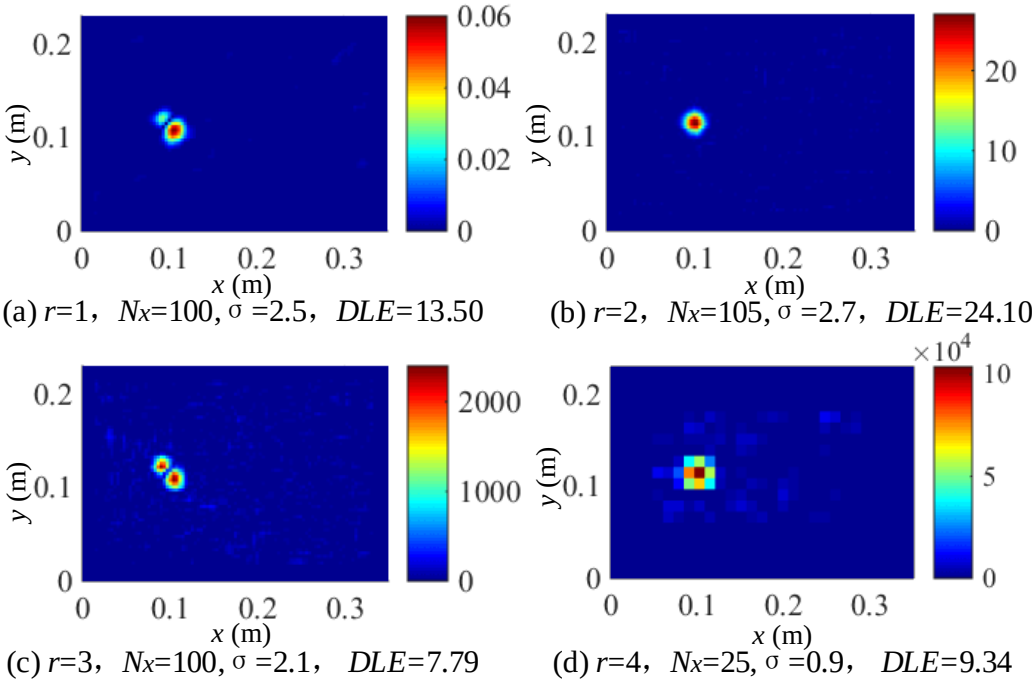

(a) r=1， Nx=100, σ =2.5， DLE=13.50 (b) r=2， Nx=105, σ =2.7， DLE=24.10

(c) r=3， Nx=100, σ =2.1， DLE=7.79 (d) r=4， Nx=25, σ =0.9， DLE=9.34

Figure 10. The best damage localization for a plate with a damage of 5% depth reduction by using $w_{\mathrm{d}}^{r}(x,y)(r=1,2,3,4)$ with 0.05% noise.

6 Experimental validation

In order to verify the proposed baseline-free adaptive damage localization method, cantilever aluminium plates with the same physical and geometrical properties as those used in the numerical study are tested. The experimental set-up is illustrated in Fig. 11. The damage is introduced by reducing the plate thickness on the other side. As shown in Figs. 5 (a) and 12, a damage zone with 10% thickness reduction is centred at (0.10m, 0.115m) with an area of 0.02×0.02 m^2. The plate is excited by a shaker (LDS V406) close to its right edge, as depicted in Fig. 12(a).

The vibration responses are measured by a PSV-500 SLV within a measured zone which is slightly smaller than the original plate dimension to avoid the effects of the boundaries. The measurement zone is of $0.326\mathrm{m} \times 0.219\mathrm{m}$ spanning from 0.0084m to 0.3334m in the x direction and from 0.0028m to 0.2218m in the y direction as shown in Fig. 12(a). A total of 141×95 measurement points are used with a grid cell size of $0.00233\mathrm{m} \times 0.00233\mathrm{m}$. Here, a sufficiently large number of measurement

points is necessary to capture the damage-induced local CDS distortions, especially for incipient damage. For practical applications outside a laboratory, the fast development of measurement technology, exemplified by the non-contact measurement technology such as optic and imaging techniques, embedded sensors and smart sensing skin technology etc., could offer improved solutions to the measurement problem in the near future. It should be understood that the proposed technique may need to be revamped to adapt to the physical quantities measured by different techniques.

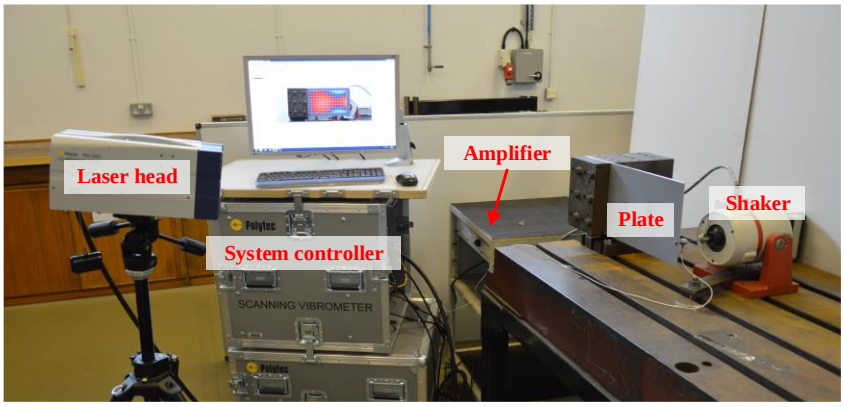

Figure 11. Experimental set-up of a cantilever plate.

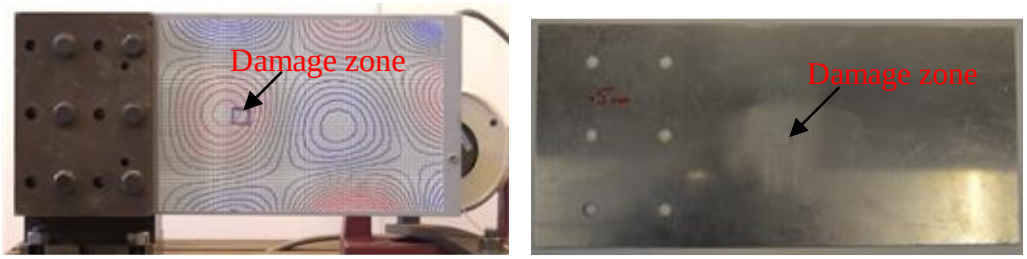

(a) (b)

Figure 12. A plate with a damage zone: (a) Front surface and (b) Back surface.

To determine the resonant frequencies of the plate, a pseudo random signal of 0-2000 Hz, generated by the PSV-500 system, is used to excite the plate. The associated mode shape data are then obtained at the resonance frequency. Certainly, the operational deflection shapes at non-resonant frequencies can also be used.

Here, the 10^{th} resonant frequency is used and the velocities of measurement grid are

acquired using the 'FastScan' mode of PSV-500, with the bandwidth of the acquisition signal being set as 300Hz. A wider bandwidth can speed-up the measurement, whereas a narrow bandwidth will provide a better signal to noise ratio. In the present case, 30 averages are used for each measurement point, amounting to a total of 141×95 measurement points.

With the measured mode shape of the damage state, damage localization is first conducted by using the mode shape and its first four order spatial derivatives without denoising, with results illustrated in Fig. 13. It can be seen that without denoising, the mode shape (r=0) provides the best damage localization results. The high-order mode shape derivatives are readily contaminated by measurement noise and unable to provide useful information for damage localization, in agreement with the numerical analyses reported above. Therefore, the proposed **DI** is robust to the experimental measurement noise in $w_{\mathrm{d}}(x, y)$ but sensitive to the propagated measurement noise in $w_{\mathrm{d}}^{r}(x, y)(r = 1,2,3,4)$.

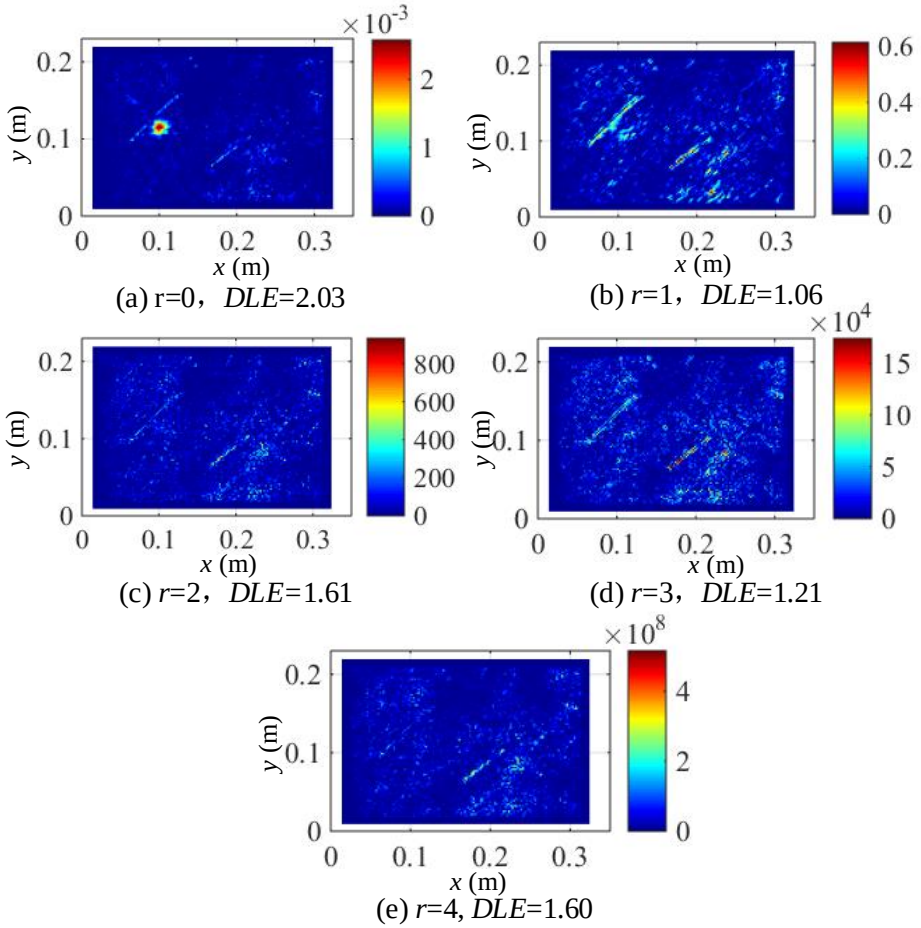

(a) r=0， *DLE*=2.03 (b) *r*=1， *DLE*=1.06

(c) *r*=2， *DLE*=1.61 (d) *r*=3， *DLE*=1.21

(e) *r*=4, *DLE*=1.60

Figure 13. Damage localization of a plate with a damage of 10% depth reduction by using $w_{\mathrm{d}}^{r}(x,y)(r=0,1,2,3,4)$.

Then, the proposed baseline-free adaptive damage localization approach is applied using $w_{\mathrm{d}}^{r}(x,y)(r=1,2,3,4)$. The DLE values using different d and σ with a damage zone of 10% and 16.67% depth reduction are presented in Fig. 14 and Fig. 15, respectively. It is seen from both figures that high DLE value zones can be obtained, which indicates that the tuning of d and σ is an efficient strategy to improve the damage localization performance. Therefore, the proposed adaptive damage localization method shows its effectiveness in obtaining more accurate damage localization results by adjusting the measurement sampling interval d and scale parameter σ of Gaussian smoothing. Moreover, $w_{\mathrm{d}}^{2}(x,y)$ provides the best damage localization results among the first four order spatial derivatives of $w_{\mathrm{d}}(x,y)$, as it possesses the largest zone of high DLE values as shown in Fig. 14(b) and Fig. 15(b). In

addition, the magnitude of DLE values are proved to be capable of indicating the relative damage severity.

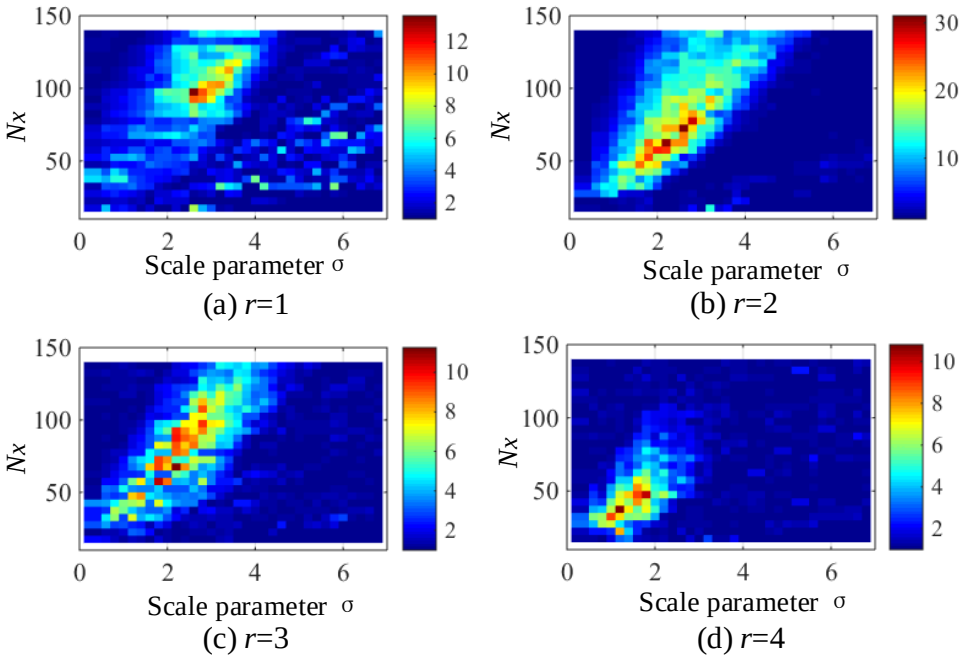

Figure 14. DLE values of $w_{\mathrm{d}}^{r}(x,y)(r=1,2,3,4)$ for a plate with a damage zone of 10% depth reduction (N_x is the number of measurement points along x direction, d=0.326/N_x and $N_y=\mathrm{round}(0.219/d)$).

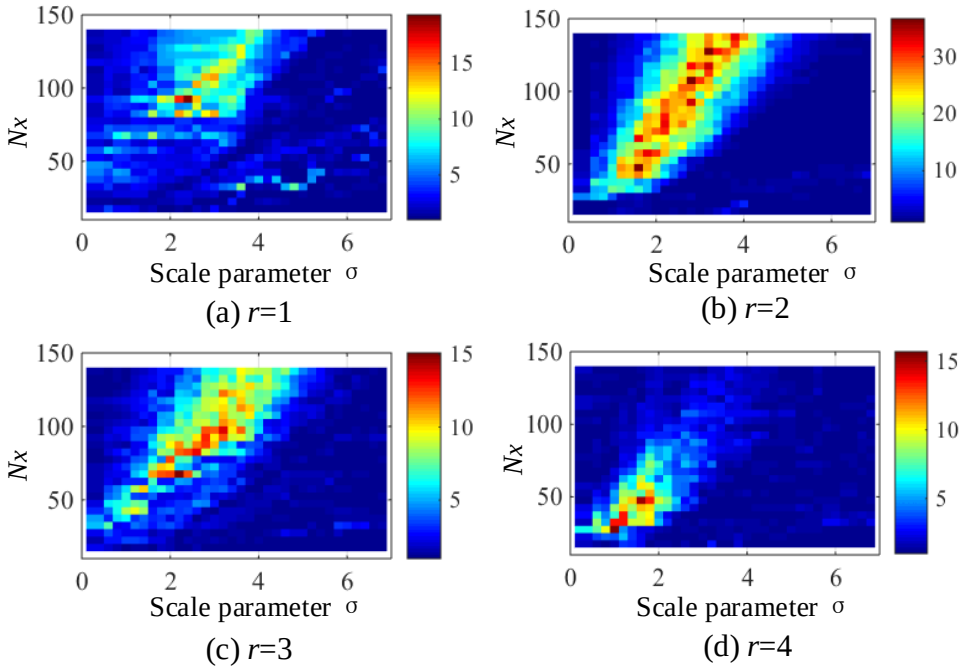

(a) r=1 (b) r=2

(c) r=3 (d) r=4

Figure 15. DLE values of $w_{\mathrm{d}}^{r}(x,y)(r=1,2,3,4)$ for a plate with a damage zone of 16.77% depth reduction (N_x is the number of measurement points along x direction, d=0.326/N_x and $N_y=\mathrm{round}(0.219/d)$).

Finally, the best damage localization results using $w_{\mathrm{d}}^{r}(x,y)(r=1,2,3,4)$ for a plate with a damage zone of 10% depth reduction are presented in Fig. 16, which correspond to the highest DLE values in Fig. 14. A comparison with Fig. 10 verifies the conclusions obtained from the numerical study. Moreover, Fig. 16 experimentally demonstrates that, with a proper choice of the sample interval d and the scale parameter σ, all first four order spatial derivatives of $w_{\mathrm{d}}(x,y)$ can provide acceptable damage localization results.

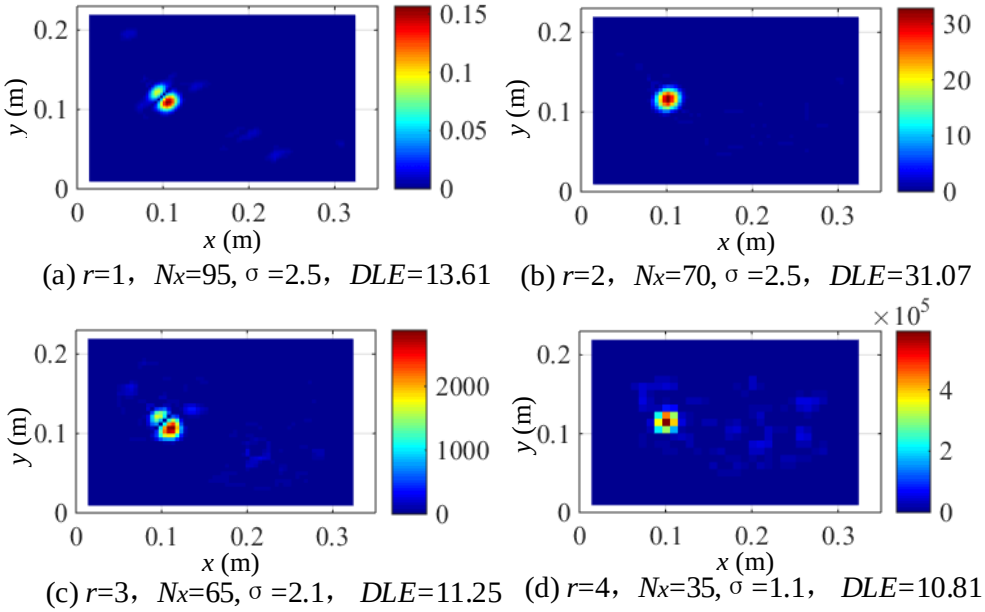

(a) r=1， Nx=95, σ =2.5， DLE=13.61 (b) r=2， Nx=70, σ =2.5， DLE=31.07

(c) r=3， Nx=65, σ =2.1， DLE=11.25 (d) r=4， Nx=35, σ =1.1， DLE=10.81

Figure 16. The best damage localization results using $w_{\mathrm{d}}^{r}(x,y)(r=1,2,3,4)$ for a plate with a damage zone of 10% depth reduction.

7 Conclusions

From both theoretical and experimental perspective, this paper investigates three vital aspects in the characteristic deflection shape (CDS) based non-destructive damage localization: suppression of measurement noise, baseline-free and adaptive damage localization. Instead of trying to determine an optimal spatial sampling interval on a trial-error basis to minimize the measurement noise and the truncation errors of the finite difference calculation, an effective parameter tuning strategy is proposed, which optimizes both the spatial sampling interval of CDS's and the scale parameter of Gaussian smoothing to achieve accurate damage localization results, quantified by a damage localization evaluator (DLE). The baseline-free damage localization index is evaluated by using the low-rank structure of 2-D CDS's (or their spatial derivatives) and the location sparsity of the damage-induced characteristics. Numerical and experimental results demonstrate that the proposed baseline-free adaptive damage localization approach is robust and effective in reducing the effects of measurement noise to obtain more accurate damage localization.

Other conclusions are summarized as follows:

1. Robust principal component analysis is shown to be effective to extract the damage-induced local characteristics of 2-D CDS's and CDS spatial derivatives.
2. The higher the order of CDS spatial derivative, the larger the magnitude of the damage-induced local shape distortions and the more susceptible it is to measurement noise.
3. The magnitude of the DLE values is capable of indicating the relative damage severity.
4. The second-order CDS spatial derivative, through a proper balancing of the damage sensitivity and anti-noise robustness, is shown to provide the best damage localization results among the first four order spatial derivatives of CDS's.

Acknowledgements

The experiments were carried out in the School of Engineering, University of Liverpool.

References

[1] X. Kong, C. Cai, J. Hu, The state-of-the-art on framework of vibration-based structural damage identification for decision making, Applied Sciences, 7 (2017) 497 (001-031).

[2] C. Zhang, L. Cheng, H. Xu, J. Qiu, Structural damage detection based on virtual element boundary measurement, Journal of Sound and Vibration, 372 (2016) 133-146.

[3] Y. Zhou, N.M.M. Maia, R.P.C. Sampaio, M.A. Wahab, Structural damage detection using transmissibility together with hierarchical clustering analysis and similarity measure, Structural Health Monitoring, 16 (2016) 711-731.

[4] N.M.M. Maia, J.M.M. Silva, E.A.M. Almas, R.P.C. Sampaio, Damage detection in structures: from mode shape to frequency response function methods, Mechanical Systems and Signal Processing, 17 (2003) 489-498.

[5] J.K. Sinha, M.I. Friswell, S. Edwards, Simplified models for the location of cracks in beam structures using measured vibration data, Journal of Sound and Vibration, 251 (2002) 13-38.

[6] C. Surace, R. Saxena, M. Gherlone, H. Darwich, Damage localisation in plate like-

structures using the two-dimensional polynomial annihilation edge detection method, Journal of Sound and Vibration, 333 (2014) 5412-5426.
[7] S. Rucevskis, R. Janeliukstis, P. Akishin, A. Chate, Mode shape-based damage detection in plate structure without baseline data, Structural Control and Health Monitoring, 23 (2016) 1180-1193.
[8] P. Cornwell, S.W. Doebling, C.R. Farrar, Application of the strain energy damage detection method to plate-like structures, Journal of Sound and Vibration, 224 (1999) 359-374.
[9] K. Roy, S. Ray-Chaudhuri, Fundamental mode shape and its derivatives in structural damage localization, Journal of Sound and Vibration, 332 (2013) 5584-5593.
[10] Y. Yan, L. Cheng, Z. Wu, L. Yam, Development in vibration-based structural damage detection technique, Mechanical Systems and Signal Processing, 21 (2007) 2198-2211.
[11] S. Cao, H. Ouyang, Robust multi-damage localisation using common eigenvector analysis and covariance matrix changes, Mechanical Systems and Signal Processing, 111 (2018) 663-677.
[12] M. Thiene, M. Zaccariotto, U. Galvanetto, Application of proper orthogonal decomposition to damage detection in homogeneous plates and composite beams, Journal of Engineering Mechanics, 139 (2013) 1539-1550.
[13] A.Z. Khan, A.B. Stanbridge, D.J. Ewins, Detecting damage in vibrating structures with a scanning LDV, Optics and Lasers in Engineering, 32 (1999) 583-592.
[14] W. Xu, M. Cao, W. Ostachowicz, M. Radzieński, N. Xia, Two-dimensional curvature mode shape method based on wavelets and Teager energy for damage detection in plates, Journal of Sound and Vibration, 347 (2015) 266-278.
[15] E. Douka, S. Loutridis, A. Trochidis, Crack identification in plates using wavelet analysis, Journal of Sound and Vibration, 270 (2004) 279-295.
[16] R. Bai, W. Ostachowicz, M. Cao, Z. Su, Crack detection in beams in noisy conditions using scale fractal dimension analysis of mode shapes, Smart Materials and Structures, 23 (2014) 065014.
[17] A. Gentile, A. Messina, On the continuous wavelet transforms applied to discrete vibrational data for detecting open cracks in damaged beams, International Journal of Solids and Structures, 40 (2003) 295-315.
[18] M. Cao, P. Qiao, Integrated wavelet transform and its application to vibration mode shapes for the damage detection of beam-type structures, Smart Materials and Structures, 17 (2008) 055014.
[19] R. Bai, W. Ostachowicz, M. Radzieński, M. Cao, Vibrational damage detection using fractal surface singularities with noncontact laser measurement, Journal of

Vibration and Control, 22 (2016) 2569-2581.
[20] P. Qiao, M. Cao, Waveform fractal dimension for mode shape-based damage identification of beam-type structures, International Journal of Solids and Structures, 45 (2008) 5946-5961.
[21] Y. Yang, S. Nagarajaiah, Dynamic imaging: real-time detection of local structural damage with blind separation of low-rank background and sparse innovation, Journal of Structural Engineering, 142 (2015) 04015144.
[22] C.P. Ratcliffe, Damage detection using a modified Laplacian operator on mode shape data, Journal of Sound and Vibration, 204 (1997) 505-517.
[23] Y. Xu, W. Zhu, Non-model-based damage identification of plates using measured mode shapes, Structural Health Monitoring, 16 (2016) 3-23.
[24] S. Cao, H. Ouyang, Robust structural damage detection and localization based on joint approximate diagonalization technique in frequency domain, Smart Materials and Structures, 26 (2017) 015005.
[25] Y. Yang, P. Sun, S. Nagarajaiah, S.M. Bachilo, R.B. Weisman, Full-field, high-spatial-resolution detection of local structural damage from low-resolution random strain field measurements, Journal of Sound and Vibration, 399 (2017) 75-85.
[26] H. Lopes, F. Ferreira, J.V. Araújo dos Santos, P. Moreno-García, Localization of damage with speckle shearography and higher order spatial derivatives, Mechanical Systems and Signal Processing, 49 (2014) 24-38.
[27] J.F. Gauthier, T.M. Whalen, J. Liu, Experimental validation of the higher-order derivative discontinuity method for damage identification, Structural Control and Health Monitoring, 15 (2008) 143-161.
[28] T.M. Whalen, The behavior of higher order mode shape derivatives in damaged, beam-like structures, Journal of Sound and Vibration, 309 (2008) 426-464.
[29] L. Montanari, A. Spagnoli, B. Basu, B. Broderick, On the effect of spatial sampling in damage detection of cracked beams by continuous wavelet transform, Journal of Sound and Vibration, 345 (2015) 233-249.
[30] G. Quaranta, B. Carboni, W. Lacarbonara, Damage detection by modal curvatures: numerical issues, Journal of Vibration and Control, 22 (2016) 1913-1927.
[31] E. Sazonov, P. Klinkhachorn, Optimal spatial sampling interval for damage detection by curvature or strain energy mode shapes, Journal of Sound and Vibration, 285 (2005) 783-801.
[32] P. Moreno-García, H. Lopes, J.A. dos Santos, Application of higher order finite differences to damage localization in laminated composite plates, Composite Structures, 156 (2016) 385-392.
[33] Z. Zhou, L.D. Wegner, B.F. Sparling, Vibration-based detection of small-scale

damage on a bridge deck, Journal of Structural Engineering, 133 (2007) 1257-1267.
[34] X. Jiang, Z. Ma, W. Ren, Crack detection from the slope of the mode shape using complex continuous wavelet transform, Computer-Aided Civil and Infrastructure Engineering, 27 (2012) 187-201.
[35] H. Lopes, R.M. Guedes, M. Vaz, An improved mixed numerical-experimental method for stress field calculation, Optics & Laser Technology, 39 (2007) 1066-1073.
[36] H. Xu, L. Cheng, Z. Su, Suppressing influence of measurement noise on vibration-based damage detection involving higher-order derivatives, Advances in Structural Engineering, 16 (2013) 233-244.
[37] N.S. Aybat, D. Goldfarb, S. Ma, Efficient algorithms for robust and stable principal component pursuit problems, Computational Optimization and Applications, 58 (2014) 1-29.
[38] T. Bouwmans, E.H. Zahzah, Robust PCA via principal component pursuit: A review for a comparative evaluation in video surveillance, Computer Vision and Image Understanding, 122 (2014) 22-34.
[39] C. Zhang, L. Cheng, J. Qiu, H. Wang, Damage detection based on sparse virtual element boundary measurement using metal-core piezoelectric fiber, Structural Health Monitoring, 17 (2018) 15-23.
[40] P. Moreno-García, J.A. dos Santos, H. Lopes, A new technique to optimize the use of mode shape derivatives to localize damage in laminated composite plates, Composite Structures, 108 (2014) 548-554.
[41] T. Lindeberg, B.M. ter Haar Romeny, Linear scale-space I: Basic theory, in: Geometry-Driven Diffusion in Computer Vision, Springer, 1994, pp. 1-38.
[42] C. Pezerat, J. Guyader, Two inverse methods for localization of external sources exciting a beam, Acta Acustica, 3 (1995) 1-10.
[43] C. Pezerat, J. Guyader, Force analysis technique: reconstruction of force distribution on plates, Acta Acustica united with Acustica, 86 (2000) 322-332.
[44] H. Xu, L. Cheng, Z. Su, J. Guyader, Damage visualization based on local dynamic perturbation: Theory and application to characterization of multi-damage in a plane structure, Journal of Sound and Vibration, 332 (2013) 3438-3462.